# Energy and exergy analysis of a multi-stage cooling cycle of scramjet to produce electricity and hydrogen

**POURIA SEYED MATIN**[1] **AND HADI GHAEBI**[2,*]

[1] *Tarbiat Modares University of Tehran, Teahran,Iran*
[2] *Department of Mechanical Engineering, Faculty of Engineering, University of Mohaghegh Ardabili, Ardabil, Iran*
[*] *Corresponding author: hghaebi@uma.ac.ir*

*Manuscript received 08 September, 2019; revised 05 January, 2020, accepted 07 January, 2020. Paper no. JEMT-1909-1196.*

**A multi-stage open cooling cycle of scramjet for electricity and hydrogen co-production is proposed in which the fuel of scramjet is used as a coolant of the cooling cycle. Thermodynamic and exergetic examinations of the advanced system have been conducted to appraise the performance of the cycle, electricity and hydrogen production. In this integral system, the waste heat of scramjet drives the power sub-cycle whilst the PEM electrolyzer input electricity is supplied by a portion of the net electricity output of the cycle. It is figured out that the multi-expansion process reveals more advantages in comparison to the single-expansion process in terms of more cooling capacity, electricity, and production. For the fuel mass flow rate of 0.4 kg/s, the cooling capacity of the new proposed cycle is computed 9.16 MW, the net electricity output is calculated about 3.38 MW and the hydrogen production rate is attained 42.16 kg/h. On the other hand, the exergetic analysis results have proved the fact that the PEM electrolyzer has the highest exergy destruction ratio by 48% among all components of the cycle. In this case, the energy and exergy efficiencies of the overall set-up are acquired by 12.95% and 22.16%, correspondingly. The outcomes of parametric evaluation demonstrated that electricity and hydrogen productions are directly proportional to the backpressure of the pump accordingly, more electricity and hydrogen are generated by higher backpressure. But, increasing the mass flow rate of fuel does not have any tangible impact on energy and exergy efficiency of the whole set-up thus both remain approximately constant.** 

***keywords:*** *Thermodynamic analysis, Scramjet, Hydrogen, Multi-expansion, M-OCC, PEM electrolyzer.*

http://dx.doi.org/10.22109/jemt.2020.200875.1196

## NOMENCLATURE

### Symbols

$C_p$ Specific heat capacity ($kJ.kg^{-1}.K^{-1}$)
**D** Membrane thickness ($\mu m$)
**E** Electrical energy ($kJ$)
**ex** Exergy rate per unit mass ($kW/kg$)
$\dot{E}x$ Exergy rate ($kW$)
**F** Faraday constant ($C/mol$)
**G** Gibbs free energy ($kJ.kmol^{-1}$)
**Gen** Generator
**H** Specific enthalpy per mole ($kJ.kmol^{-1}$)
**h** Specific enthalpy per mass ($kJ.kg^{-1}$)
**J** Current density ($A.m^{-2}$)
$J_a^{ref}$ Pre-exponential factor of anode ($A.m^{-2}$)
$J_c^{ref}$ Pre-exponential factor of cathode ($A.m^{-2}$)
$J_i^{ref}$ Pre-exponential factor ($A.m^{-2}$)
**LHV** Lower heating value ($kJ.kg^{-1}$)
$\dot{m}$ Mass flow rate ($kg.s^{-1}$)
$\dot{m}_0$ Mass flow rate of fuel ($kg.s^{-1}$)
$\dot{N}$ Molar mass flow rate ($kmol.s^{-1}$)
**P** Pressure ($MPa$)
**Q** Heat transfer energy ($kJ$)
$\dot{Q}$ Heat transfer rate ($kW$)
**R** PEM ohmic resistance ($\Omega$)
**S** Specific entropy per mole ($kJ.kmol^{-1}.K^{-1}$)
**s** Specific entropy per mass ($kJ.kg^{-1}.K^{-1}$)
**T** Temperature ($K$)
$V_0$ Reversible potential ($V$)
$V_{act,a}$ Activation over-potential of anode ($V$)

$V_{act,c}$ Activation over-potential of cathode ($V$)
$V$ Electrical potential ($V$)
$w$ Specific power per mass unit ($MW/kg$)
$\dot{W}$ Power rate ($kW$)
$x$ Distance in membrane ($m$)
$Y_{D,i}$ Exergy destruction ratio of the ith component (%)
$y_i$ Concentration
$z_t$ Purchased-equipment cost of turbine ($)

### Acronyms

**EES** Engineering Equation Solver
**HE** Heat exchanger
**M-OCC** Multi-stage OCC
**OCC** Open cooling cycle
**PEM** Proton exchange membrane
**RCC** Regenerative cooling cycle

### Greek Symbols

$\eta$ Efficiency (%)
$\delta$ Multiplication ratio
$\phi$ Reduction ratio
$\rho$ Density ($kg.m^{-3}$)
$\gamma$ Heat capacity ratio
$\lambda(x)$ Local ionic conductivity ($\Omega^{-1}$)
$\pi$ Pressure ratio

### Subscripts and superscripts

$a$ Anode
$act,a$ Activation of anode
$act,c$ Activation of cathode
$av$ Average
$c$ Cathode
$CH$ Chemical
$CP$ Cooling passage
$cr$ Critical
$D$ Destruction
$en$ Energy
$ex$ Exergy
$F$ Fuel
$G$ Generator
$i$ $i^{th}$ component
$int$ Intermediate
$in$ Inlet
$is$ Isentropic
$j$ $j^{th}$ stage
$KN$ Kinetic
$net$ Net value
$out$ Outlet
$P$ Pump
$PH$ Physical
$PT$ Potential
$ref$ Reference
$scr$ Scramjet
$t$ Turbine

## 1. INTRODUCTION

There great interest in air breathing propulsion vehicles has been traced back many decades ago. In the continuing effort to get more applicable access to supersonic vehicles due to their ability to uphold high-speed atmospheric flight, supersonic combustion ramjets (scramjets) have been proposed to be studied [1–3]. One of the key issues of scramjet technology is the thermal management of scramjet because of the high heat release level in the scramjet combustion chamber. The heat flux density of scramjet is ranged between 0.5 and 2.5 MW per unit area of the combustion chamber for the wall temperature of 500-2000 K at a flight Mach number of 8 [4]. In such a high temperature, not only the conventional known materials but also the most developed composite substances could not endure and operate properly [5].

Various approaches are devised for the cooling purpose in such conditions in which among all, using a regenerative cooling cycle (RCC) has been commonly regarded as one of the most viable solutions [6, 7]. By this method, the heat absorption capacity of the fuel is utilized to cool the scramjet earlier than entering the combustion chamber, but limited heat absorption capacity of fuel aboard cannot supply the whole cooling needs of the scramjet, adequately. In hydrogen-fueled scramjets, the flow rate of fuel coolant will exceed the stoichiometric flow rate during the flight at a speed above a certain Mach number [8]. In other words, more fuel than the mission requisite should be conveyed by the scramjet due to the low heat sink of the fuel [9, 10]. Accordingly, Qin et al [8] advanced an open cooling cycle (OCC) of scramjet engines as a scientific and feasible solution of increasing fuel heat sink without accretion in the fuel flow rate. In their system, the high-temperature output coolant of the first cooling passage is cooled down to be reused in the second cooling process. For reducing the temperature of the fuel (as coolant), a turbine is installed to produce the power as well. This process can be repeated several times, which is called multi-OCC (M-OCC). In this scenario, the heat absorption capacity of the fuel is successively used thus the required flow rate of the fuel will be reduced. In a theoretical study, a multiple re-cooled cycle of a scramjet is proposed to investigate the performance and characteristics of the system and is compared with RCC [11]. However, the wasted heat recovery provides a good opportunity for electricity extraction. Bao et al [12] have studied the power generation and heat sink improvement of M-OCC in hydrogen-fueled scramjet. Their results showed the power generation of 500 as well as high heat sink improvement which is obtained by utilizing the M-OCC. Successively using several turbines leads to more power generation. This is the main concept behind the employment of multi-expansion cooling systems in this study.

Meanwhile, ancillary set-ups used in hypersonic vehicles, including fuel injection, circuit measuring, and tracking controller systems require a great deal of electrical power [13]. Thus, for hypersonic vehicles, it is necessary to provide an energy recovery set-up to meet its surplus power needs [12].

Several studies have proposed new configurations of recovery systems for power generation via high-temperature thermal heat of the scramjets. Zhang et al [14] evaluated the performance of a new power generation system for waste energy recovery of a scramjet in which a vapor turbine is used to drive the generator. For the turbine working pressure ratio of 5 and an inlet temperature of 940 K, the generated power is calculated 100 kJ per unit of fuel mass flow rate. Li and Wang [15] proposed a theoretical model integrating a thermoelectric generator (TEG)

with a RCC to produce power from the temperature difference between cooling channel walls. Through this layout, their system produced 61.69 kW electricity with overall exergy efficiency of about 22% for the fuel flow rate of 0.4 kg/s. In another similar research, a novel power/refrigeration cogeneration system has been proposed by Cheng et al [16] applicable to waste heat extraction from hypersonic vehicles. The proposed power generation system consisted of a three-stage TEG and a closed Brayton cycle (CBC). They found that decoupling heating and cooling set-up is more appealing for the matching purpose of two cold and heat sources.

Hydrogen has superior performance in comparison with all kinds of carbon-based fuels (hydrocarbon fuels) due to its higher ignitability, greater flame stability, high diffusivity for mixing enhancement, high heat capacity (among all gases) and low dynamic viscosity which, all in all, provide better cooling characteristics at high combustion temperatures and flight speeds [17–19]. In addition, the use of hydrogen as fuel, in hypersonic propulsion systems (at M>5), has no competitor for long-range transportation applications [20].

Burning 0.36 kg of liquid combusting with air produces 3.21 kg of and some [21], underlining the fact that some water can be stored for different applications (some portion of this produced water is used later in this study for the water supply of hydrogen production via a waste heat recovery process). Despite the fact that hydrogen is usually stored in cryogenic conditions at high volume in comparison with kerosene [20], Brewer [22] stated that using liquid in aircraft is highly efficacious due to its low operating cost in comparison with kerosene. Corchero et al [23] deduced that the specific fuel consumption of fueled Tupolev Tu-324/414 jet regional aircraft is 2.8 times lower than that of the kerosene-based aircraft, leading to the increase of the engine life. Therefore, hydrogen can be widely used in space propulsion systems such as space launchers. The technical feasibility, environmental compatibility, safety and economic aspects of using as fuel in aviation are more highlighted in the CRYOPLANE project of the European Commission launched in 2000 [20]. Another example of hydrogen utility as fuel in aviation was demonstrated in 2013 in which Phantom Eye aircraft fueled by hydrogen reached an altitude of 28,000 ft and speed of 115 km/h for approximately 4.5 hours of flight [20]. They have planned to install a 90 kW fuel cell into an A320 by 2015. In conclusion, it is noteworthy to pinpoint that any provision of surplus hydrogen via waste thermal heat of the combustion process in scramjet can be an encouraging solution to provide some portion of the required input of different fuel cells. This deliberation is the main idea behind the present study since the waste heat of the scramjet set-up is used for supplying some portion of hydrogen fuel of the scramjet or other aforementioned applications within the plane.

$H_2$ production process is predominantly carrying out by biomass conversion, steam methane reforming or water splitting methods. Splitting water is a thermochemical process which is called electrolysis. There are three common forms of electrolyzing procedures consisting of the oxidation of solid, alkaline and PEM electrolysis. Hydrogen production via PEM electrolysis has numerous advantages particularly in the renewable energy framework such as low environmental impact, being compact, containing no hazardous chemicals, producing high pure hydrogen, etc. [24]. PEM electrolyzer is the most prevalent method for hydrogen production in energy systems applicable for low-grade heat sources due to its high compatibility and is introduced as the commendable hydrogen production method for future utilities [25–27]. Leung et al [28] performed thermodynamic and exergy studies of a PEM electrolyzer showing that hydrogen production and energy efficiency improvement are significantly related to the PEM working temperature, electrode catalytic activity, and electrolyte wall thickness. Marangio et al [29] presented a model for the theoretical study of the PEM cells in which a complicated pattern of ohmic losses in electrodes and membrane was developed. In another research work, carried out by Ahmadi et al [30], a solar-driven PEM electrolyzer has been assimilated with an OHEC (ocean heat energy conversion) system to extract. Energy and exergy analyses have been conducted in their proposed model and it is discovered that the extracted hydrogen is 1.2 kg/h with thermodynamic and exergy efficiency of 3.6% and 23%, respectively.

According to the aforementioned literature review, it can be said that there is no deliberation on the cogeneration of power/hydrogen from waste heat of the cooling channel of a scramjet set-up, up to now. Thus, it is imperious to produce power and hydrogen simultaneously for the required demands in hypersonic vehicles. It is self-evident that extracting the surplus amount of power and via electrolysis process from the waste thermal heat of a scramjet seems to be a suitable resolution to tackle high fuel consumption issues in the scramjet initiation. However, no comprehensive investigation regarding this concept of electricity/hydrogen cogeneration is presented, up to yet while it is highly important to cover this shortcoming by proposing a basic configuration for the model.

The aim of the present work is to advance a novel multi-stage OCC for electricity/hydrogen cogeneration besides cooling the scramjet. Additionally, a thoroughgoing study on multi-expansion effects is accomplished from thermodynamic standpoint. In the proposed set-up, the PEM is driven by a portion of net output power production of the proposed system whilst the waste heat of scramjet is as heat source of the multi cooling cycle. Overall, the novelties of present study can be highlighted as:

- A novel multi-generation open cooling cycle of scramjet for electricity/hydrogen cogeneration has been proposed.
- Energy and exergy analysis have been accomplished to investigate the feasibility and performance of the proposed cycle.
- A comprehensive parametric study of some important parameters has been conducted.

## 2. CYCLE DESCRIPTION

An illustrative configuration of the novel proposed set-up has been depicted in Fig. 1. The system includes two main sub-cycles, power and PEM electrolyzer sub-cycle. The liquid hydrogen is pumped from the scramjet fuel tank to the first cooling passage entry (state 2). Whilst, $H_2$ constantly streams across the cooling passage rapidly turning to a supercritical gas by absorbing the heat of scramjet engine in which fuel works as a coolant. Then the superheated hydrogen enters the first turbine (state 3) and the hydrogen, under an isentropic condition, is expanded to produce electric power by the help of coupled generator. Through this process, $H_2$ is cooled down to $T_4$ (state 4). The cooled coolant is heated up above the supercritical condition by flowing through the second cooling passage (process 4 to 5) and again is cooled down by being expanded through turbine 2 (process 5 to 6). The process of heating the coolant to cool the combustion chamber and cooling it down through turbine to

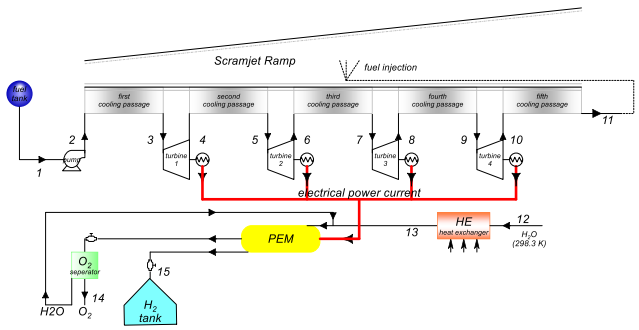


**Fig. 1.** Schematic diagram of the proposed novel scramjet multi-stage OCC coupled with a PEM electrolyzer.

produce the electricity accomplishes two time more in the third and fourth cooling passages and two turbines (turbine 3 and turbine 4) have been placed in outlets of this two cooling passages. Eventually, the last cooling process (process 10-11) occurs in the fifth cooling passage. Then the hydrogen leaves cooling cycle (state11) and can be injected into the combustion chamber, as fuel. The electrolyzing process in PEM, for hydrogen production, requires electric power and heat. The electricity is supplied by M-OCC sub-system and heat comes from the waste heat of scramjet combustion chamber, as shown in Fig. 1. Meanwhile, to bring the water up to the PEM temperature it first goes through the heat exchanger (HE) at state 12, before entering to the PEM (state 13). In electrolyzing process, $H_2$ began to leave the cathode side by a fair segment of the generated net electricity and cool down to the ambient temperature (state 15). On the anode side, $O_2$ separation from the water content occurs. The $O_2$ gas is cooled to ambient temperature and accumulated to the storage tank (state 14). The residual water content of the electrolyzer is recirculated by a water sub-supply pipeline for the next $H_2$ producing cycle. By carrying on the process sequentially, the $H_2$ will be produced and stored in a tank.

## 3. PRESUMPTIONS AND METHODOLOGY

### A. Presumptions

The following presumptions are made:

- Steady-state mathematical models
- The specific heat is considered to be constant
- The coolant is considered to be perfect gas after the first cooling passage
- There are no pressure losses through pipelines and connections
- In turbines, there are no heat transfer losses
- The reference temperature is considered to be 298 K
- The reference pressure is considered to be 0.101 MPa
- Scramjet body temperature is considered to be constant and equal to scramjet body average temperature
- Water enters the PEM electrolyzer at 353 K
- There are no energy losses in electrolyzing process

The presumptions are not precise enough in order to get actual design. Although, they are sufficient for the aim of this study.

### B. Some basic definitions of performance criteria

The reduction of the fuel (as coolant) flow rate for cooling by improving the heat sink capacity per unit of fuel is the main purpose of OCC. Some parameters are needed to be defined for bringing into comparison the performance privileges of the multi-stage OCC and regenerative cooling cycles.

#### *B.1. Multiplication ratio of the fuel heat absorption ($\delta$)*

If the $Q_i$ is considered to be the cooling load of the first cooling passage and $Q_{i+1}$ cooling load of the second cooling passage, multiplication ratio is defined as a parameter by which the cooling capacity improvement of each cooling passage stage in comparison with its previous stage can be assessed [8]. According to above definition, the multiplication ratio can be obtained as:

$$\delta_i = Q_{i+1} \Big/ \sum_{m=1}^{i} Q_m \tag{1}$$

Where, i=1,2,3,4 which stand for second, third, fourth and fifth cooling passages, respectively.

#### *B.2. Reduction ratio of mass flow rate of fuel for cooling ($\phi$)*

The augmentation of fuel heat absorption capacity is interpreted as reduction in the mass flow rate of fuel (as coolant). In the other words, the straight impact of utilizing OCC in cooling system performance is to reduce the required fuel flow rate. In order to evaluate the capability of OCC in decreasing fuel flow rate, a reduction ratio of OCC should be defined. Thus, the reduction ratio can be calculated as:

$$\phi_i = Q_{i+1} \Big/ \sum_{m=1}^{i+1} Q_m \tag{2}$$

As mentioned above, i=1,2,3,4 which stand for second, third, fourth and fifth cooling passages, respectively

### C. PEM electrolyzer formulae

An illustrative configuration of the PEM electrolyzer sub-cycle is located in the bottom part of Fig. 1, as it can be observed. The PEM electrolyzer produce hydrogen by water splitting process, an electrochemical reaction in which the electricity and heat are utilized as energy suppliers. Hence, an electrochemical based modeling is required to appraise the PEM from thermodynamic and exergy prospects.

The summation of needed thermal energy ($T\Delta S$) and $\Delta G$ (Gibb's free energy) of reaction attains the overall energy requirement [30], as below:

$$\Delta H = \Delta G + T\Delta S \tag{3}$$

The $H_2$ molar mass flow rate is calculated by [30]:

$$\dot{N}_{H_{2out}} = \frac{J}{2F} = \dot{N}_{H_2O,reacted} \tag{4}$$

$F$ is the Faraday constant and $J$ is called the current density. The electrical power entrance rate to the electrolyzer is derived as [30]:

$$E_{electric} = JV \tag{5}$$

The voltage potential (V) is given as:

$$V = V_0 + V_{act,a} + V_{act,c} + V_{ohm} \tag{6}$$

Where, $V_0$ is the reversible potential and is extracted by the Nernst equation as below:

$$V_0 = 1.229 - 8.5 \times 10^{-4} \left(T_{PEM} - 298\right) \tag{7}$$

Here, $V_{act,c}$, $V_{act,a}$, and $V_{ohm}$ are the cathode activation over-potential, the anode activation over-potential and the ohmic over-potential of the electrolyte, respectively. The ionic conductivity at each region of the PEM membrane $\lambda(x)$ is calculated as:

$$\sigma_{PEM}\left[\lambda\left(x\right)\right] = \left[0.5139\lambda\left(x\right) - 0.326\right] \exp\left[1268\left(\frac{1}{303} - \frac{1}{T}\right)\right] \quad (8)$$

Where, $x$ is the distance calculated from the cathode side surface. $\lambda(x)$ is calculated as follows [30]:

$$\lambda\left(x\right) = \frac{\lambda_a - \lambda_c}{D}x + \lambda_c \quad (9)$$

$\lambda_a$ and $\lambda_c$ represent the water quantity of anode and cathode membranes at their own surfaces, respectively. $D$ is the membrane thickness. The PEM ohmic resistance is expressed as [28]:

$$R_{PEM} = \int_0^D \frac{dx}{\sigma_{PEM}\left[\lambda\left(x\right)\right]} \quad (10)$$

The ohmic over-potential equation based on the Ohm's potential law is defined as follow [28]:

$$V_{ohm\ ,PEM} = JR_{PEM} \quad (11)$$

The activation over-potential ($V_{act,i}$) is given by [30]:

$$V_{act,i} = \frac{RT}{F}\sinh^{-1}\left(\frac{J}{2J_{a,i}}\right),\ i = a,c \quad (12)$$

Here, $J_0$ is the exchange current density of the electrolyzer obtained from Eq. (13) as well as, $a$ and $c$ indexes indicate the anode and cathode sides, respectively [28]:

$$J_{0,i} = J_i^{ref} \exp\left(-\frac{E_{act,i}}{RT}\right),\ i = a,c \quad (13)$$

$E_{act,i}$ is the activation electricity of PEM (for both anode and cathode sides) and $J_i^{ref}$ is called the pre-exponential factor of function.

### D. Thermodynamic analysis

In this section, thermodynamic modeling and some other mathematical relations of the devised system are explained in details. Each component of the system is regarded as a control volume. The general forms of mass and energy balance equations for a control volume at steady state can be expressed as [31]:

$$\sum \dot{m}_{in} = \sum \dot{m}_{out} \quad (14)$$

$$\dot{Q} - \dot{W} = \sum \dot{m}_{out}h_{out} - \sum \dot{m}_{in}h_{in} \quad (15)$$

The energy efficiency of the recommended cycle is obtained by summing the produced hydrogen energy and net electricity as outputs of the cycle divided by input energy as below:

$$\eta_{en} = \frac{LHV_{H_2}.\dot{m}_{15} + (1-\eta_G).\dot{W}_{net}}{\dot{Q}_{total}} \quad (16)$$

$LHV_{H_2}$ is lower heating value of $H_2$ which is assumed 120.211 $kJ/kg$ [31]. $\dot{Q}_{total}$ is the total cooling of the scramjet used as heat source of the system and its calculation is explained in Table 1. Considering a turbine working under an isentropic process between states $b$ and $c$ and without any loss of power due to mechanical friction (Fig. 2), its outlet temperature can be achieved as [31]:

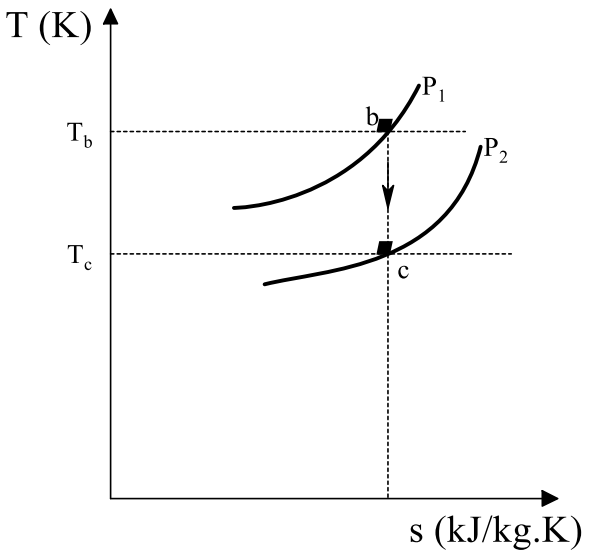


**Fig. 2.** T-s diagram of an isentropic expansion process in a turbine.

$$T_c = T_b\left\{1 - \eta_t\left[1 - \pi^{(1-\gamma)/\gamma}\right]\right\} \quad (17)$$

$\pi$ is the pressure ratio defined as ratio of inlet and outlet pressures of the turbine:

$$\pi = \frac{p_b}{p_c} \quad (18)$$

Table 1 has listed some of the significant thermodynamic equations based on energy balance relation.

**Table 1.** Energy balance equations for each component of the simulated set-up

| Parameters | Equation |
|---|---|
| Heat load of $i^{th}$ cooling passage | $\dot{Q}_i = \dot{m}_i.C_p.(T_{2i+1} - T_{2i})$ |
| Specific work of $i^{th}$ turbine | $w_{ti} = \eta_t C_p T_{2i+1}\left[1 - \pi_i^{(1-\gamma)/\gamma}\right]$ |
| Specific work of pump | $w_p = \frac{P_2 - P_1}{\eta_p \rho_1}$ |
| Specific net power | $w_{net} = \sum_{i=1}^{4} w_{ti} - w_p$ |
| Net electricity | $\dot{W}_{net} = \dot{m}_0.w_{net}$ |
| Heat load of heat exchanger | $Q_{HE} = \dot{m}_w.(h_{13} - h_{12})$ |
| Total cooling | $\dot{Q}_{total} = \sum_{i=1}^{5} \dot{Q}_i + \dot{Q}_{HE}$ |
| | |

The rate of total exergy of a flow ($\dot{E}x_{total}$) consists of four main components: physical exergy rate ($\dot{E}x_{PH}$), kinetic exergy rate ($\dot{E}x_{KN}$), potential exergy rate ($\dot{E}x_{PT}$) and chemical exergy rate ($\dot{E}x_{CH}$) [32]:

$$\dot{E}x_{total} = \dot{E}x_{PH} + \dot{E}x_{KN} + \dot{E}x_{PT} + \dot{E}x_{CH} \quad (19)$$

Among these four components, kinetic and potential exergies are usually negligible due to their small values. The rate of physical exergy of a closed system is given as below:

$$\dot{E}x_{Ph} = \dot{m}\,(h - h_0 - T_0(s - s_0)) \quad (20)$$

Also, for chemical exergy rate we have:

$$\dot{E}x_{ch} = \dot{m}\left[\sum_{i=1}^{n} x_i ex_{ch,i} + RT_0 \sum_{i=1}^{n} x_i \ln x_i\right] \quad (21)$$

In which, $y_i$ is the molar concentration and $ex_{CH,i}$ shows the specific chemical exergy of the material.

The exergy balance equation for the ith component of a system can be stated as [32]:

$$\dot{E}x_F^i = \dot{E}x_P^i + \dot{E}x_D^i \quad (22)$$

$\dot{E}x_D^i$ is the rate of exergy destruction and $\dot{E}x_D^F$ and $\dot{E}x_D^P$ are exergy rates of fuel and product of the ith component, respectively. In the same way, the balance equation for the overall system can be considered as:

$$\dot{E}x_F^{total} = \dot{E}x_P^{total} + \dot{E}x_D^{total} \quad (23)$$

Exergetic efficiency of element $i$ ($\eta_{ex}^i$) is expressed as:

$$\eta_{ex}^i = \dot{E}x_P^i \Big/ \dot{E}x_F^i \quad (24)$$

To compare the exergetic destruction of each component of the system with other components, the exergy destruction ratio is defined as follows [32]:

$$y_{D,i} = \dot{E}x_{D,i} / \dot{E}x_{D,total} \quad (25)$$

The total exergetic efficiency of the system can be considered same as Eq. (25):

$$\eta_{ex}^{total} = \dot{E}x_P^{total} \Big/ \dot{E}x_F^{total} \quad (26)$$

Table 2 provides some of the important exergy based balance equations of the introduced system.

## 4. RESULTS AND DISCUSSION

An appropriate EES code, based on Section 3 mentioned assumptions, has been developed to analyze the system from energetic and exergetic prospects. In order to run the simulation code and obtain the outputs, some input data are needed. Table 3 listed the reliable input parameters to simulate the cycle [5, 8, 14]. Additionally, Table 4 listed some other input data for simulation of the PEM electrolyzer. By running developed code, some key parameters of the flow have been gained (Table 5) as outcome of this simulation. These thermodynamic parameters consist of temperature, pressure, mass flow, enthalpy, entropy and exergy rates at each state.

### A. Model validation

To evaluate the accuracy of our simulation, two sub-systems from literature have been validated. In the first case, a scramjet set-up is selected [8] and a PEM electrolyzer is selected as the second scenario [30]. The validation results of OCC and PEM are shown in Table 6 and Fig. 3, respectively. Fig. 3 shows the variation of cell potential of PEM with current density for present work and Ahmadi et al study. In Table 6 the magnitude of multiplication ratio ($\delta$), reduction ratio ($\phi$) and produced net power ($w_{net}$) in different back pressures of pump ($P_2$) was listed. Accordingly, the validation results indicate a great agreement with two reports and some the trivial difference can be occurred by calculation error of computer and operator or approximation errors in constant and inputs.

**Table 3.** Some of the required input data for simulation of the system

| Parameter | value |
|---|---|
| Back pressure of pump, $P_2(MPa)$ | 22 |
| Average temperature of scramjet body, $T_{av}(K)$ | 1000 |
| Scramjet combustion chamber pressure, $P_{11}(MPa)$ | 1 |
| Fuel tank temperature, $T_1(K)$ | 25 |
| Fuel tank pressure, $P_1(MPa)$ | 0.24 |
| Mass flow rate of fuel, $\dot{m}_0(kg/s)$ | 0.4 |
| Mass flow rate of PEM entrance water, $\dot{m}_{12}(kg/s)$ | 0.0311 |
| PEM entrance water temperature, $T_{12}(K)$ | 298 |
| PEM temperature, $T_{PEM}(K)$ | 353 |
| Turbine efficiency, $\eta_t$ | 0.8 |
| Pump efficiency, $\eta_P$ | 0.7 |
| Generator power efficiency, $\eta_G$ | 0.65 |

**Table 4.** Input parameters are used to model the PEM [31]

| Parameter | value |
|---|---|
| $P_{O_2}(MPa)$ | 0.1 |
| $P_{H_2}(MPa)$ | 0.1 |
| $T_{PEM}(K)$ | 353 |
| $E_{act,a}(KJ/mol)$ | 76 |
| $E_{act,c}(KJ/mol)$ | 18 |
| $\lambda_a(\Omega^-1)$ | 14 |
| $\lambda_c(\Omega^-1)$ | 10 |
| $D(\mu m)$ | 100 |
| $J_c^{ref}(A/m^2)$ | $1.7 * 10^5$ |
| $J_a^{ref}(A/m^2)$ | $4.6 * 10^3$ |
| $F(C/mol)$ | 96486 |

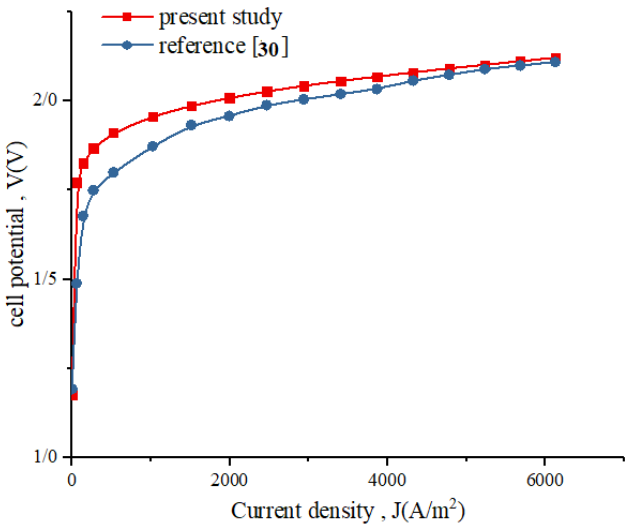


**Fig. 3.** The PEM electrolyzer model validation of present study with reference [30].

### B. Thermodynamic analysis results

The thermodynamic modelling results have been presented in this section. The developed code conducted by input data to

**Table 2.** Exergy equations of main components of the simulated system

| Component | Exergy of fuel | Exergy of product | Exergy of destruction | Exergetic efficiency | Exergy destruction ratio |
|---|---|---|---|---|---|
| $i^{th}$ Cooling passage | $\dot{E}x_{F,i} = \dot{Q}i\left(1-\frac{T_0}{T_{ref-scr}}\right)$ | $\dot{E}x_{P,Q1} = \dot{E}x_3 - \dot{E}x_2$ | $\dot{E}x_{D,Q1} = \dot{E}x_{F,Q1} - \dot{E}x_{P,Q1}$ | $\eta_{ex,Qi} = \frac{\dot{E}x_{P,Qi}}{\dot{E}x_{F,Qi}}$ | $y_{D,Qi=}\frac{\dot{E}x_{D,Qi}}{\dot{E}x_{D,total}}$ |
| $i^{th}$ Turbine | $\dot{E}x_{F,ti} = \dot{E}x_{2i+1} - \dot{E}x_{2i+2}$ | $\dot{E}x_{P,ti} = \dot{m}_i.w_{ti}$ | $\dot{E}x_{D,ti} = \dot{E}x_{F,ti} - \dot{E}x_{P,ti}$ | $\eta_{ex,ti} = \frac{\dot{E}x_{P,ti}}{\dot{E}x_{F,ti}}$ | $y_{D,ti=}\frac{\dot{E}x_{D,ti}}{\dot{E}x_{D,total}}$ |
| Pump | $\dot{E}x_{F,p} = \dot{m}_1.w_p$ | $\dot{E}x_{P,p} = \dot{E}x_2 - \dot{E}x_1$ | $\dot{E}x_{D,p} = \dot{E}x_{F,p} - \dot{E}x_{P,p}$ | $\eta_{ex,p} = \frac{\dot{E}x_{P,p}}{\dot{E}x_{F,p}}$ | $y_{D,p} = \frac{\dot{E}x_{D,p}}{\dot{E}x_{D,total}}$ |
| PEM | $\dot{E}x_{F,PEM} = \eta_G.\dot{W}_{net}$ | $\dot{E}x_{P,PEM} = \dot{E}x_{15} + \dot{E}x_{16}$ | $\dot{E}x_{D,PEM} = \dot{E}x_{F,PEM} - \dot{E}x_{P,PEM}$ | $\eta_{ex,PEM} = \frac{\dot{E}x_{P,PEM}}{\dot{E}x_{F,PEM}}$ | $y_{D,PEM} = \frac{\dot{E}x_{D,PEM}}{\dot{E}x_{D,total}}$ |
| Heat exchanger | $\dot{E}x_{F,HE} = Q_{HE}\left(1-\frac{T_0}{T_{ref-HE}}\right)$ | $\dot{E}x_{P,HE} = \dot{E}x_{13} - \dot{E}x_{12}$ | $\dot{E}x_{D,HE} = \dot{E}x_{F,HE} - \dot{E}x_{P,HE}$ | $\eta_{ex,HE} = \frac{\dot{E}x_{P,HE}}{\dot{E}x_{F,HE}}$ | $y_{D,HE} = \frac{\dot{E}x_{D,HE}}{\dot{E}x_{D,total}}$ |

**Table 5.** Thermodynamic properties in each state of the simulated system

| State | Fluid | T(K) | P (MPa) | $\dot{m}(kg/s)$ | $h(kJ/kg)$ | $s(kJ/kg.K)$ | $\dot{E}x(kW)$ |
|---|---|---|---|---|---|---|---|
| 1 | Hydrogen | 25 | 0.24 | 0.4 | 479.4 | 20.25 | 2510 |
| 2 | Hydrogen | 54.9 | 22 | 0.4 | 579.8 | 20.25 | 2551 |
| 3 | Hydrogen | 1000 | 22 | 0.4 | 14387 | 48.83 | 4758 |
| 4 | Hydrogen | 714.4 | 4.69 | 0.4 | 10010 | 50.22 | 2846 |
| 5 | Hydrogen | 1000 | 4.69 | 0.4 | 14235 | 55.19 | 3959 |
| 6 | Hydrogen | 841.5 | 2.166 | 0.4 | 11856 | 55.81 | 2936 |
| 7 | Hydrogen | 1000 | 2.166 | 0.4 | 14213 | 58.38 | 3581 |
| 8 | Hydrogen | 916.4 | 1.472 | 0.4 | 12959 | 58.67 | 3045 |
| 9 | Hydrogen | 1000 | 1.471 | 0.4 | 14207 | 59.97 | 3393 |
| 10 | Hydrogen | 916.4 | 1 | 0.4 | 12954 | 60.26 | 2859 |
| 11 | Hydrogen | 1000 | 1 | 0.4 | 14202 | 61.57 | 3207 |
| 12 | Water | 290 | 0.101 | 0.0321 | 70.75 | 0.251 | 77.51 |
| 13 | Water | 353 | 0.101 | 0.0321 | 334.3 | 1.073 | 78.31 |
| 14 | Oxygen | 353 | 0.101 | 0.0929 | 50.36 | 0.156 | 12.04 |
| 15 | Hydrogen | 353 | 0.101 | 0.01171 | 4720 | 55.81 | 2.379 |

**Table 6.** Validation results for OCC sub-system between current study and Ref. [8]

| Performance parameters | Back pressure of pump, $P_2$ (MPa) | | | | | | | | | | | |
|---|---|---|---|---|---|---|---|---|---|---|---|---|
| | 3 | | 5 | | 10 | | 15 | | 20 | | 24 | |
| | Present study | Qin et al | Present study | Qin et al | Present study | Qin et al | Present study | Qin et al | Present study | Qin et al | Present study | Qin et al |
| $\delta(\%)$ | 27.63 | 27.63 | 37.81 | 37.81 | 49.44 | 49.44 | 55.25 | 55.25 | 58.99 | 58.99 | 61.2 | 61.2 |
| $\phi(\%)$ | 21.65 | 21.65 | 27.43 | 27.43 | 33.08 | 33.08 | 35.59 | 35.59 | 37.1 | 37.1 | 37.96 | 37.96 |
| $W_{net}(MW/kg)$ | 3.947 | 3.891 | 5.4 | 5.305 | 7.062 | 6.866 | 7.892 | 7.596 | 8.425 | 8.03 | 8.741 | 8.266 |

calculate the required parameters and the energy outcomes of the introduced cycle, listed in Table 7. For mass flow rate of 0.4 (kg/s), the produced net electricity is 3386 (kW) and hydrogen production is 42.14 (kg/h) when the 65% of produced electricity be reachable for PEM as the power input. The overall energy efficiency of proposed system in which the electricity and hydrogen are as products, is about 13.07%. The energy efficiency of the system is supposed to be good enough by consideration of using low-grade heat source (waste heat), as we know low-grade heat sources have low efficiencies. The cooling capacity of proposed system is 9.16 MW. It can be figured out that the proposed cooling cycle is suitable for a scramjet with average wall temperature of 1000 *K*, at 8 much flight condition in which the heat flux per unit area of wall is about 1.3 MW per unit of wall area. The hydrogen production quantity is noteworthy in comparison with other similar system. Such high hydrogen production systems would have numerous usages in aerospace industry.

The results of exergy study have been obtained as presented in Table 8. The overall system exergy efficiency is 22.16 %. The PEM electolyzer with relative exergy destruction ratio of more than 47% (Fig. 4) has the least exergy efficiency, among all components the system. This high level of exergy destruction is engendered by irreversibility of chemical reaction (water electrolyzing process) [33]. After the PEM electrolyzer, the first cooling passage has the highest exergy destruction with more than 37% of exergy destruction ratio of overall destruction and this is because of very high temperature difference that heat transferring occurs in it. The exergy destruction is in direct proportion to temperature difference [33]. These two high destruction rate components of system are clearly shown in Fig. 4. These main sources of exergy destruction can be considered to have more efficient system.

Producing power and hydrogen, simultaneously, integrated with cooling system not only meats the cooling and accessory energy needs in Scramjet but also improves the performance of hypersonic vehicles which has great capability in doing various missions. It can be said that the cooling system with waste energy recovery system is a promising solution for energy commitments of scramjet technology to overcome the challenges and

**Table 7.** Energy evaluation results obtained from simulation

| parameter | Value |
|---|---|
| First cooling passage heat load, $\dot{Q}_1(kW)$ | 5523 |
| Second cooling passage heat load, $\dot{Q}_2(kW)$ | 1690 |
| Third cooling passage heat load, $\dot{Q}_3(kW)$ | 942.5 |
| Fourth cooling passage heat load, $\dot{Q}_4(kW)$ | 499.2 |
| Fifth cooling passage heat load, $\dot{Q}_5(kW)$ | 499.2 |
| Pump power, $W_p(MJ/kg)$ | 0.4353 |
| Turbine 1 power, $W_t1(MJ/kg)$ | 4.158 |
| Turbine 2 power, $W_t2(MJ/kg)$ | 2.308 |
| Turbine 3 power, $W_t3(MJ/kg)$ | 1.217 |
| Turbine 4 power, $W_t4(MJ/kg)$ | 1.217 |
| Net electricity output, $\dot{W}_{net}(kW)$ | 3386 |
| PEM power entrance, $\dot{W}_G(kW)$ | 2201 |
| Hydrogen production, $\dot{m}_{H_2}(kg/h)$ | 42.14 |
| PEM heat exchanger load, $\dot{Q}_{HE}(kW)$ | 8.461 |
| Total cooling, $\dot{Q}_{total}(kW)$ | 9162 |
| Energy efficiency overall system, $\eta_{en}(\%)$ | 12.95 |
| Multiplication ratio of second cooling passage, $\delta_1$ | 0.3022 |
| Multiplication ratio of third cooling passage, $\delta_2$ | 0.1086 |
| Multiplication ratio of fourth cooling passage, $\delta_3$ | 0.0398 |
| Multiplication ratio of fifth cooling passage, $\delta_4$ | 0.03978 |
| Reduction ratio of second cooling passage, $\phi_1$ | 0.2321 |
| Reduction ratio of third cooling passage, $\phi_2$ | 0.07544 |
| Reduction ratio of fourth cooling passage, $\phi_3$ | 0.029968 |
| Reduction ratio of fifth cooling passage, $\phi_4$ | 0.02967 |

**Table 8.** Exergy study results of proposed cycle

| Component | $\dot{E}x_F(kW)$ | $\dot{E}x_P(kW)$ | $\dot{E}x_D(kW)$ | $\eta_{ex}(\%)$ | $Y_D(\%)$ |
|---|---|---|---|---|---|
| First cooling passage | 3921 | 2207 | 1714 | 56.28 | 37.23 |
| Second cooling passage | 1200 | 1113 | 86.63 | 92.78 | 1.882 |
| Third cooling passage | 669.4 | 645.2 | 24.2 | 96.38 | 0.5256 |
| Fourth cooling passage | 354.4 | 348 | 6.403 | 98.19 | 0.1391 |
| Fifth cooling passage | 354.4 | 348 | 6.403 | 98.19 | 0.131 |
| Pump | 174.1 | 40.14 | 134 | 23.05 | 2.91 |
| Turbine 1 | 1912 | 1663 | 284.6 | 87 | 5.399 |
| Turbine 2 | 1024 | 923.1 | 100.5 | 90.18 | 2.182 |
| Turbine 3 | 535.3 | 487 | 48.28 | 90.98 | 1.049 |
| Turbine 4 | 534.5 | 487 | 47.5 | 91.11 | 1.032 |
| PEM | 2201 | 14.42 | 2187 | 0.6551 | 47.49 |
| PEM heat exchanger | 1.883 | 0.8046 | 1.078 | 42.74 | 0.02341 |
| Overall system | 6501 | 1440 | 5061 | 22.16 | - |

make them more practicable. Especially when a portion of consumed fuel is supplied which is astonishing in hydrogen fueled scramjets. Based on the present study results, the proposed system hydrogen production is more than 42 kg/h. However, the present study showed an encouraging about suppling scramjet fuel by waste energy recovery systems.

## C. Parametric study

In the present part the impacts of some significant parameters on the important outputs of our system have been investigated. The mass flow rate of fuel, back pressure of pump, scramjet body temperature and generator power efficiency are chosen to be studied because these parameters had the most significant

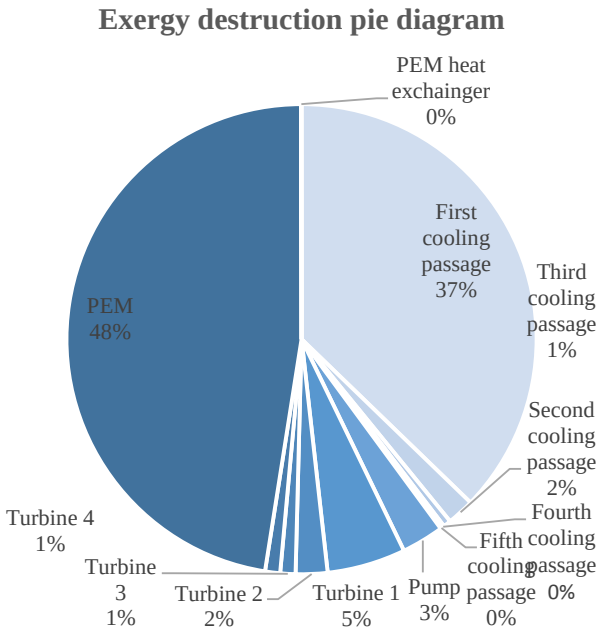


**Fig. 4.** Exergy destruction distribution of system components.

effects on the system.

### *C.1. The impact of mass flow rate of fuel on the system*

In Fig. 5, the effects of mass flow rate of the scramjet fuel on the net electricity output, total cooling, hydrogen production as well as energy and exergy efficiencies have been shown. Scramjet cooling, electricity and hydrogen production increase when mass flow rate of fuel increases (Fig. 5.a), in advanced set-up. As we know, the electricity production and heat absorption of cooling passages have direct proportion to mass flow rate of fuel. Due to mass flow rate augmentation when the flow energy difference (flow enthalpy difference) of states has remained constant and specific heat capacity which is considered to be constant in temperature range of the system, the electricity production and cooling have liner increasing trend. The electricity production increment in power sub-cycle that a segment of produced electricity drives the PEM electrolyzer sub-cycle, cause to a rise in current density of electrolyzer. Therefore the $H_2$ production will increase, regarding Eq. (4). The energy and exergy efficiencies of the whole cycle are approximately constant in spite of any variation in the mass flow rate. This can be reasonable by considering this matter that mass flow rate augmentation results in higher electricity and hydrogen production. However, as it can be observed, the absorbed heat of cooling passages which is the heat sources of proposed system also rises in the same scale of productions. Therefore, the energy and exergy efficiencies remain about constant, as drawn in Fig. 5.b. In scramjet due to some existent limitations, paying attention to the mass flow rate effects in designing more practical scramjets can be significant.

### *C.2. The impact of pump back pressure on the system*

The effects of pump back pressure on the main output parameters of system are shown in Fig. 6. The electricity output and the amount of scramjet cooling go up by pump back pressure increment, Fig. 6.a. The increment of back pressure of pump means expansion ratio increment, higher pressure drop and higher tem-

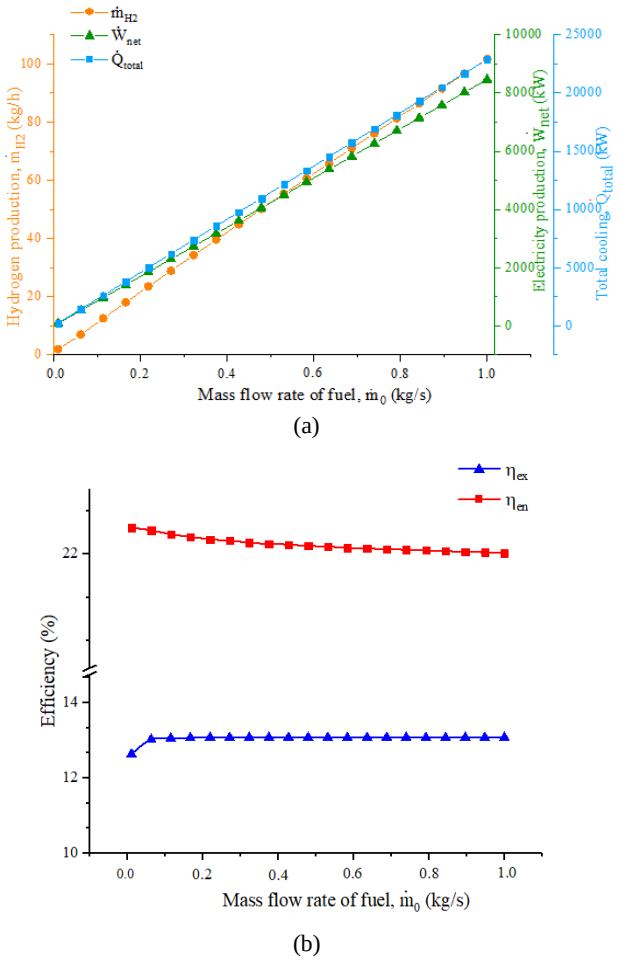


**Fig. 5.** The impact of the mass flow rate of fuel on: (a) net electricity production, hydrogen production and total cooling, (b) exergy and energy efficiencies.

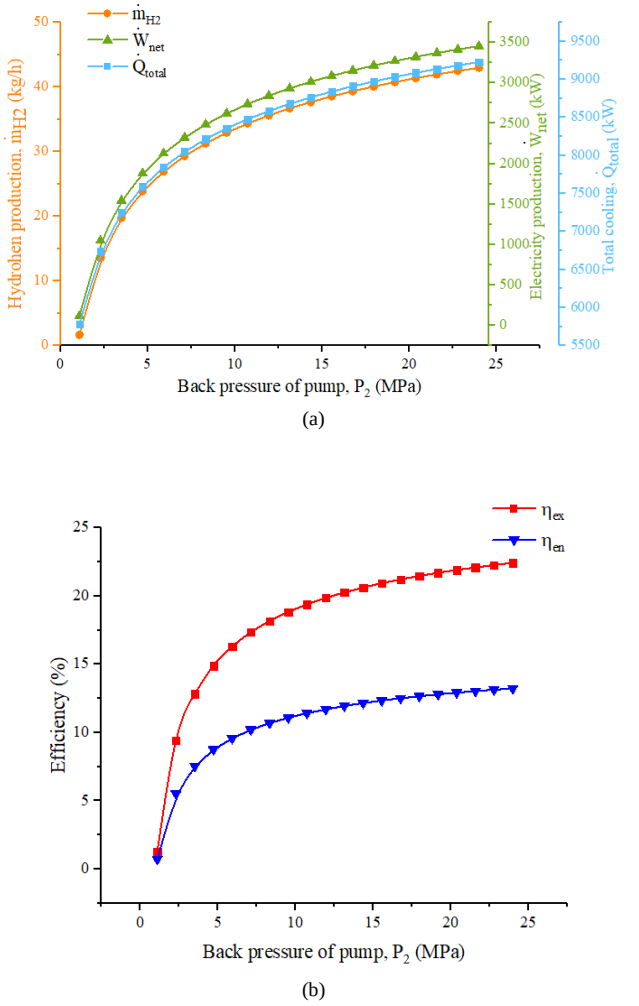


**Fig. 6.** The pump back pressure effect on: (a) the hydrogen and net electricity production and (b) the energy and exergy efficiencies.

perature drop through expansion process. The power relation of turbine tells that the power production has direct relevance with expansion ratio. On the other hand, higher temperature difference is equal to higher heat transferring (based upon heat transfer principles). Accordingly, an increase in back pressure, in constant mass flow rate and constant specific heat capacity, cause to more electricity production and cooling capacity. As mentioned above, the electricity production increment leads to more hydrogen production and more hydrogen production means more optimized system for scramjet. Also the total cooling (that is heat source of cycle) and two production parameters of system both increase but the augmentation rate of production is sensibly more and results in energy and exergy efficiency improvements, as Fig. 7.b represents.

### *C.3. The impact of scramjet body temperature on the system*

Increasing the scramjet body temperature shows a growing behavior on the three main outputs of system including, the cooling load, electricity and hydrogen production, as presented in Fig. 7.a. Higher scramjet body temperature means higher enthalpy of fuel coolant at the outlets of cooling passages (the inlets of turbines) and we know that electricity production and cooling process (heat transfer) are in direct proportional with enthalpy difference thus both will show increasing behavior with body temperature increasing at which the mass flow rate of fuel and specific heat capacity are constant. On the other hand, increasing electricity production cause to hydrogen production increase, as explained in previous sections. As a result of scramjet body temperature increasing, both main efficiencies (energy and exergy efficiencies) of the system do not change sensibly. Considering that the cooling heat absorption increment rate which is the main heat source of the cycle, the resultant product increments rate is approximately the same scale, Fig. 7.b.

### *C.4. The effect of generator power efficiency ($\eta_G$) on the hydrogen production*

The portion of generated electricity of system that is available for PEM electrolyzer as power entrance is determined by generator power efficiency ($\eta_G$). The effect of $\eta_G$ on the hydrogen production is depicted in Fig. 8. As it can be observed, the hydrogen production rate augments reasonably when $\eta_G$ increases. As a matter of fact, the higher $\eta_G$ means higher PEM electrolyzer entrance power which leads to hydrogen production increase accordingly.

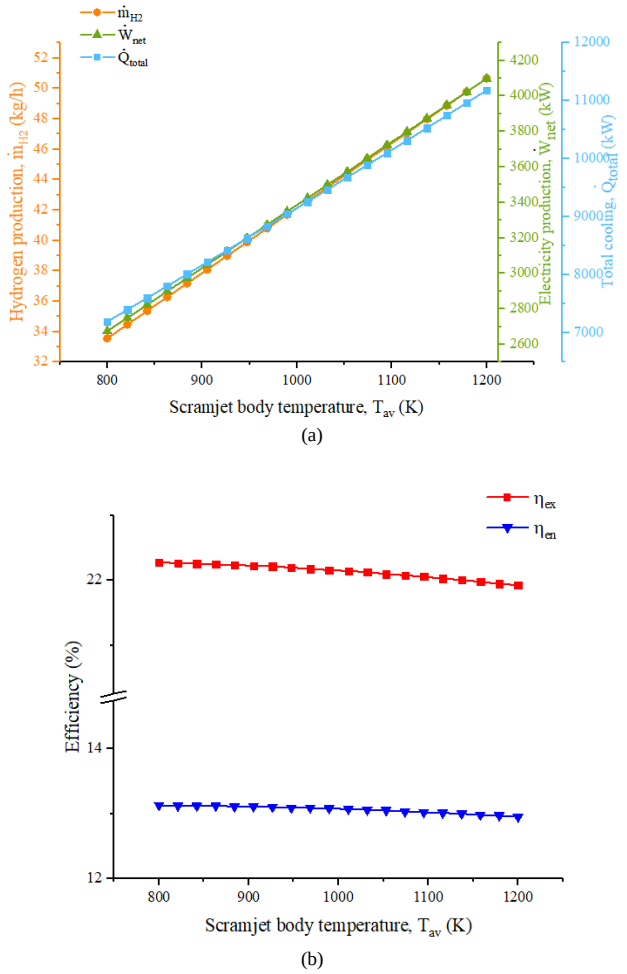


**Fig. 7.** The scramjet body temperature variation effects on: (a) the hydrogen and electricity production as well as cooling load, (b) the energy and exergy efficiencies.

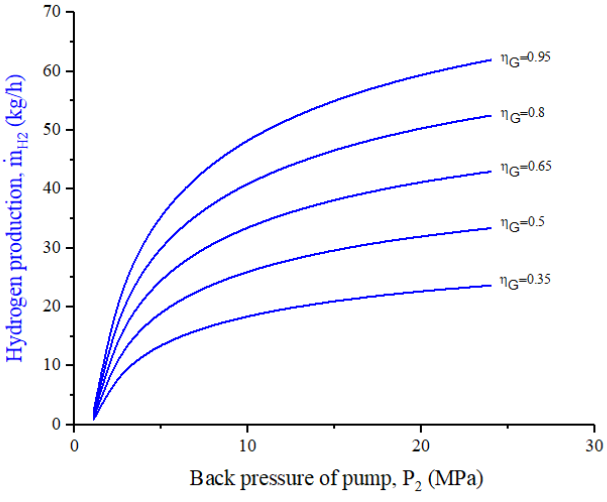


**Fig. 8.** The impact of generator power efficiency on the $H_2$ production rate in back pressure of pump variation range.

## 5. CONCLUSIONS

In this study, a M-OCC has been introduced to produce electricity and hydrogen (by employing PEM electrolyzer) alongside the main purpose of scramjet body cooling. The power production sub-section is driven by waste heat of scramjet and a distinct portion of produced net electricity is employed to drive the PEM electrolyzer. Energetic and exergetic investigation of the advanced set-up and multi-expansion effects study have been accomplished to evaluate the operation of the system. The better thermodynamic based system the more practicable scramjet can be presented. Moreover, an exhaustive parametric investigation on some important thermodynamic parameters of proposed cycle has been carried out to have better understanding of its operation. The selected parameters (average scramjet body temperature mass flow rate of fuel and back pressure of the pump) are controllable under fight condition such as flight Mach number, flight height and whole set-up consideration. Moreover, these parameters have chosen because had the most significant impacts on the system. In the present study, just some reliable amounts are given to these parameters based on some authorized scientific studies' results such as Ref. [8], Ref. [14]. Some remarkable results can be outlined as follow:

- The net electricity production, cooling load of scramjet and hydrogen production are estimated as: 3386 (kW), 9162 (kW) and 42.14 (kg/h), correspondingly.
- The overall energy and exergy efficiencies of developed system are gained 12.95 % and 22.16 %, sequentially.
- The exergy investigation results demonstrate that PEM electrolyzer has the maximum exergy destruction rate by 47.49 % and the first cooling passage has the second rank by about 38 %. These two great destructions steam from two main resources of irreversibility of systems, chemical reaction and high temperature difference.
- The electricity and hydrogen productions and total cooling capacity are increased when mass flow rate of fuel, back pressure of pump and scramjet body temperature increase.
- The energy and exergy performances of cycle remain approximately constant with increasing of the mass flow rate of fuel whereas improved with pump back pressure increment and the scramjet body temperature variation does not have any tangible effects on the whole energy and exergy efficiencies of the cycle.

## REFERENCES

1. W. H. Heiser and D. T. Pratt, Hypersonic airbreathing propulsion. Aiaa, 1994.
2. E. T. Curran, "Scramjet engines: the first forty years," Journal of Propulsion and Power, vol. 17, no. 6, pp. 1138-1148, 2001.
3. Q. Yang, J. Chang, and W. Bao, "Thermodynamic analysis on specific thrust of the hydrocarbon fueled scramjet," Energy, vol. 76, pp. 552-558, 2014.
4. P. Gerlinger and Y. H. Simsont, "Numerical investigation of scramjet strut injector cooling for different fuel mass fluxes and strut material properties at mach 8 flight conditions," Acta Astronautica, vol. 160, pp. 353-364, 2019.
5. X. Li and Z. Wang, "Exergy analysis of integrated TEG and regenerative cooling system for power generation from the scramjet cooling heat," Aerospace Science and Technology, vol. 66, pp. 12-19, 2017.
6. J. Zuo, S. Zhang, J. Qin, W. Bao, and N. Cui, "Performance evaluation of regenerative cooling/film cooling for hydrocarbon fueled scramjet engine," Acta Astronautica, vol. 148, pp. 57-68, 2018.
7. P. Xie and X. Zhang, "Hydrogen flow and heat transfer characteristic analysis in cooling channel wall with the spherical convexity structure," International Journal of Hydrogen Energy, vol. 44, no. 31, pp. 16991-17003, 2019.

8. J. Qin, W. Bao, W. Zhou, and D. Yu, "Performance cycle analysis of an open cooling cycle for a scramjet," Proceedings of the Institution of Mechanical Engineers, Part G: Journal of Aerospace Engineering, vol. 223, no. 6, pp. 599-607, 2009.
9. T. Kanda, G. Masuya, and Y. Wakamatsu, "Propellant feed system of a regeneratively cooled scramjet," Journal of Propulsion and Power, vol. 7, no. 2, pp. 299-301, 1991.
10. B. Youn and A. Mills, "Cooling panel optimization for the active cooling system of a hypersonic aircraft," Journal of thermophysics and heat transfer, vol. 9, no. 1, pp. 136-143, 1995.
11. W. Bao, J. Qin, W. Zhou, and D. Yu, "Parametric performance analysis of multiple re-cooled cycle for hydrogen fueled scramjet," international journal of hydrogen energy, vol. 34, no. 17, pp. 7334-7341, 2009.
12. W. Bao, J. Qin, W. Zhou, D. Zhang, and D. Yu, "Power generation and heat sink improvement characteristics of recooling cycle for thermal cracked hydrocarbon fueled scramjet," Science China Technological Sciences, vol. 54, no. 4, pp. 955-963, 2011.
13. K. Cheng et al., "Performance assessment of an integrated power generation and refrigeration system on hypersonic vehicles," Aerospace Science and Technology, vol. 89, pp. 192-203, 2019.
14. D. Zhang, J. Qin, Y. Feng, F. Ren, and W. Bao, "Performance evaluation of power generation system with fuel vapor turbine onboard hydrocarbon fueled scramjets," Energy, vol. 77, pp. 732-741, 2014.
15. Z. W. Xinchun Li, "Exergy analysis of integrated TEG and regenerative cooling system for power generation from the scramjet cooling heat," Aerospace Science and Technology, vol. 66, pp. 12-19, 2017.
16. K. Cheng et al., "Performance assessment of a closed-recuperative-Brayton-cycle based integrated system for power generation and engine cooling of hypersonic vehicle," Aerospace Science and Technology, vol. 87, pp. 278-288, 2019.
17. H. Li, Y. Chen, Z. Wang, T. Zhang, and Y. Li, "Study on steady state control schedule and characteristic calculation of hydrogen-fueled scramjet," in AIAA Propulsion and Energy 2019 Forum, 2019.
18. H. Wang, Z. Wang, M. Sun, and H. Wu, "Combustion modes of hydrogen jet combustion in a cavity-based supersonic combustor," International journal of hydrogen energy, vol. 38, no. 27, pp. 12078-12089, 2013.
19. F. T. Strauss, S. General, C. Manfletti, and S. Schlechtriem, "Flow Path and Interaction Analysis in a Hydrogen Transpiration Cooled Scramjet Model Combustor," in AIAA Propulsion and Energy 2019 Forum, 2019.
20. D. Cecere, E. Giacomazzi, and A. Ingenito, "A review on hydrogen industrial aerospace applications," International journal of hydrogen energy, vol. 39, no. 20, pp. 10731-10747, 2014.
21. İ. Yılmaz, M. İlbaş, M. Taştan, and C. Tarhan, "Investigation of hydrogen usage in aviation industry," Energy conversion and management, vol. 63, pp. 63-69, 2012.
22. G. Brewer, "The prospects for liquid hydrogen fueled aircraft," International Journal of Hydrogen Energy, vol. 7, no. 1, pp. 21-41, 1982.
23. G. Corchero and J. Montanes, "An Approach to the use of hydrogen for commercial aircraft engines," Proceedings of the Institution of Mechanical Engineers, Part G: Journal of Aerospace Engineering, vol. 219, no. 1, pp. 35-44, 2005.
24. Z. Abdin, C. Webb, and E. M. Gray, "Modelling and simulation of a proton exchange membrane (PEM) electrolyser cell," international journal of hydrogen energy, vol. 40, no. 39, pp. 13243-13257, 2015.
25. E. Akrami, A. Nemati, H. Nami, and F. Ranjbar, "Exergy and exergoeconomic assessment of hydrogen and cooling production from concentrated PVT equipped with PEM electrolyzer and LiBr-H2O absorption chiller," International Journal of Hydrogen Energy, vol. 43, no. 2, pp. 622-633, 2018.
26. F. A. Boyaghchi, M. Chavoshi, and V. Sabeti, "Multi-generation system incorporated with PEM electrolyzer and dual ORC based on biomass gasification waste heat recovery: exergetic, economic and environmental impact optimizations," Energy, vol. 145, pp. 38-51, 2018.
27. H. Kianfard, S. Khalilarya, and S. Jafarmadar, "Exergy and exergoeconomic evaluation of hydrogen and distilled water production via combination of PEM electrolyzer, RO desalination unit and geothermal driven dual fluid ORC," Energy conversion and management, vol. 177, pp. 339-349, 2018.
28. M. Ni, M. K. Leung, and D. Y. Leung, "Energy and exergy analysis of hydrogen production by a proton exchange membrane (PEM) electrolyzer plant," Energy conversion and management, vol. 49, no. 10, pp. 2748-2756, 2008.
29. F. Marangio, M. Santarelli, and M. Cali, "Theoretical model and experimental analysis of a high pressure PEM water electrolyser for hydrogen production," International Journal of Hydrogen Energy, vol. 34, no. 3, pp. 1143-1158, 2009.
30. P. Ahmadi, I. Dincer, and M. A. Rosen, "Energy and exergy analyses of hydrogen production via solar-boosted ocean thermal energy conversion and PEM electrolysis," International Journal of Hydrogen Energy, vol. 38, no. 4, pp. 1795-1805, 2013.
31. Y. A. Cengel and M. A. Boles, "Thermodynamics: an engineering approach," Sea, vol. 1000, p. 8862, 2002.
32. A. Bejan, G. Tsatsaronis, and M. Moran, "Thermal Design and Optimization John Wiley and Sons," Inc. New York, 1996.
33. T. J. Kotas, The exergy method of thermal plant analysis. Elsevier, 2013.